Third International Symposium on Marine Propulsors
smp'13, Launceston, Tasmania, Australia, May 2013

Prediction of the Unsteady Cavitating Performance of Ducted Propellers Subject to an Inclined Inflow

Spyros A. Kinnas[1], Chan-Hoo Jeon[1], Jay Purohit[1] & Ye Tian[1]

[1] Ocean Engineering Group, Department of Civil, Architectural and Environmental Engineering
The University of Texas at Austin, Austin, TX 78712, USA

ABSTRACT

The performance of a ducted propeller subject to uniform and inclined inflow is studied by using a hybrid method that couples a potential flow solver with a viscous fluid flow solver. In addition, by using a wall transpiration model, a boundary layer solver is interactively coupled with a three dimensional panel method in a stripwise manner to include the effects of fluid viscosity on the duct. The wall transpiration model is validated in the case of open ducts by comparing the results with those from high resolution RANS simulations. An extension scheme is applied for modification of blunt trailing edge of ducts and results are presented for open duct and duct in presence of the propeller. The results of the numerical methods are compared with experimental measurements.

Keywords

Ducted propeller Performance, Uniform/inclined inflow, Cavitation, BEM, Boundary layer solver, Trailing edge modification.

1 INTRODUCTION

The hybrid method coupling the potential flow solver (MPUF-3A) and the viscous fluid solver is developed by the Ocean Engineering Group at the University of Texas at Austin. This method takes the strong points of those two solvers and is able to simulate the ducted propeller efficiently with high accuracy. Kerwin et al. (1994) came up with the method coupling Vortex Lattice Method with Reynolds-Averaged Navier-Stokes solver to investigate the performance of ducted propellers. Hughes et al. (1992) applied a lifting surface theory and a panel method to consider the duct geometry effectively. Kinnas et al. (2004; 2009) applied the hybrid method to podded and ducted propellers. This hybrid method requires an interface tool that evaluates time-averaged body force and the effective wake. Kinnas et al. (2012_1; 2012_2) introduced the interface tool (PF2NS) and the under-relaxation scheme that prevents the performance diverged and makes the hybrid method converge rapidly during the iteration process. We also apply the hybrid method to a ducted propeller under inclined uniform inflow. The results are qualitatively reasonable.

To include the effect of viscosity in panel methods, generally a skin friction coefficient value is assumed to model the viscous shear stress, and empirical viscous pitch correction is used to approximate the influence of the boundary layer (Kerwin and Lee 1987). Since the values are selected empirically there is a need to develop a rational approach that includes the effect of fluid viscosity without having to solve for RANS. For this reason viscous-inviscid interactive methods have come up and become popular. The integral boundary layer formulation allows for the computation of quantities like displacement thickness, edge velocity and skin friction coefficient.

Viscous-inviscid interactive methods in two dimensions have been developed in the past few decades. Drela and Giles (1987) implemented a viscous-inviscid interactive solver XFOIL for 2D airfoils by coupling inviscid solution obtained from stream function approach to an integral boundary layer solver. For 3D propeller blades, Hufford et al. (1994) proposed a method of coupling the 2-D boundary layer solver used in XFOIL with a 3-D potential based panel method program for propeller flow. He assumed that the boundary layer grows only along the streamwise direction and the boundary layer variables should be negligible in the radial direction of the blade. The 2D boundary layer solver was applied separately to each strip along the constant radius of the blade. Sun (2008) coupled a perturbation potential based panel code, PROPCAV, with XFOIL considering boundary layer variables in one direction only, but further simplified that the panels of the strips were two dimensional. However, the interaction among individual strips was not taken into consideration. Kinnas et al. (2012_3) proposed a scheme to include the interactions among different strips in an iterative manner. Purohit (2013) corrected the formulation by including added interaction effects between the individual strips. In this paper the corrected formulation has been presented. Also the viscous-inviscid interactive method has been applied for a 3-D axisymmetric case by modifications in the 2-D formulation. The scheme has then been validated using open duct and by comparing the results from high resolution RANS simulations.

It is well known that potential theory cannot handle flows along ducts with blunt trailing edge accurately. A scheme

for the extension of the duct was used by Pan (2009) and Yu (2012). The approach is to model the flap shape as a second order polynomial. The extension is required to maintain continuity of slope at the point where it merges with the actual shape. A similar extension scheme has been used here with the addition of one parameter but now it has been applied for the case of ducts. The parameters of the extension scheme are systematically changed in such a way that the pressures on the lower and upper sides at the actual trailing edge location are equal. For the case of ducted propellers, since the pressures on each strip of the duct will be different due to the action of the propeller blade, the extension scheme is applied on the circumferentially averaged pressure on the duct. The detailed description of the method is given in Purohit (2013).

In this paper the viscous-inviscid coupling is also validated for ducts with blunt trailing edge by modifying the trailing edge using the extension scheme and applying the interactive scheme for calculation of viscous pressures and boundary layer variables. The results have been compared to RANS simulations

2 FORMULATION

2.1 Coupling Interface Tool : PF2NS

In order to couple the potential flow solver(MPUF-3A) with the viscous fluid flow solver, the interface tool named PF2NS (Potential Flow to Navier-Stokes) has been developed. It consists of two parts: body force (PF2NS_BF) and effective wake (PF2NS_EFF).

As shown in the figure 1, PF2NS_BF calculates time-averaged body force from the data of pressure and area that come from the potential flow solver. This body force can be added to the momentum equations as source terms. In general, the mesh of the viscous fluid flow solver has much denser than that of the potential flow solver and thus the body force data need to be interpolated when they are imported to the viscous fluid flow solver. Kinnas et al. (2012) introduced the Conservation Interpolation Scheme (CIS). This scheme provides the interpolated body force with high accuracy.

PF2NS_EFF evaluates the effective wake that subtracts propeller induced velocity from total velocity. The total velocity is the result of the viscous fluid flow solver and the propeller induced velocity can be obtained from the potential flow solver. The evaluated effective wake will be used as the inflow condition of the next iteration. This coupling procedure continues until the performances are converged. Kinnas et al.(2012) reported that this coupling could have the converged results before the 6th iteration.

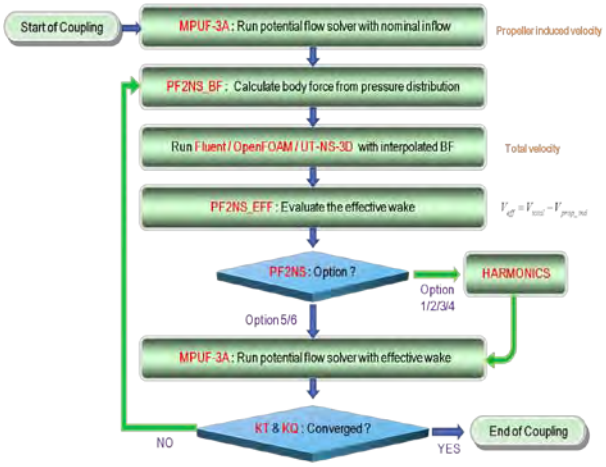

Figure 1. Coupling flowchart of potential/viscous solvers.

The PF2NS includes six options as described in Table 1. These options can be classified by dimension and location where the effective wake is evaluated. Three options are designed for the axisymmetric case and other three are for the three dimensional case. Each dimensional option has three different options. One is located at the straight line (or plane) upstream. Another is set to curved line (or plane) spaced equally from the leading edge of the propeller. The other is that the effective wake is calculated at the control points located inside the propeller zone.

Table 1. Options of the PF2NS interface tool

Dimension	Option	Location where the effective wake is evaluated
Axisymmetric (3X)	1	Straight line upstream
	3	Curve spaced equally from the leading edge of the propeller
	5	Control points inside the propeller zone
3-dimensional (3D)	2	Plane upstream
	4	Curved plane spaced equally from the leading edge of the propeller
	6	Control points inside the propeller zone

Figures 2 and 3 show the schematic diagrams of the PF2NS options. Figure 2 represents the options for the axisymmetric case and Figure 3 is the example of the option 6 (3D).

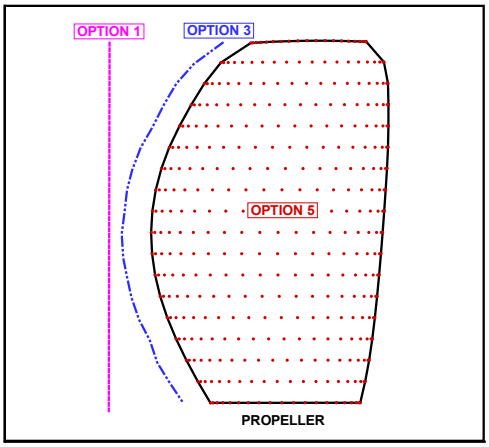

Figure 2. PF2NS options for axisymmetric cases.

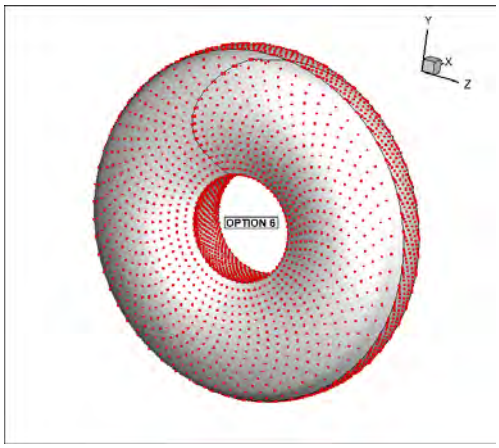

Figure 3. PF2NS option (6) for 3-dimensional cases.

2.2 Wall Transpiration Model in 2D

The inviscid and viscous flows are strongly coupled through the wall transpiration model. For 2D case as shown in Fig. 4, blowing sources with unknown strength are added on the control points of the body and the wake to simulate the effects of the viscous boundary layer.

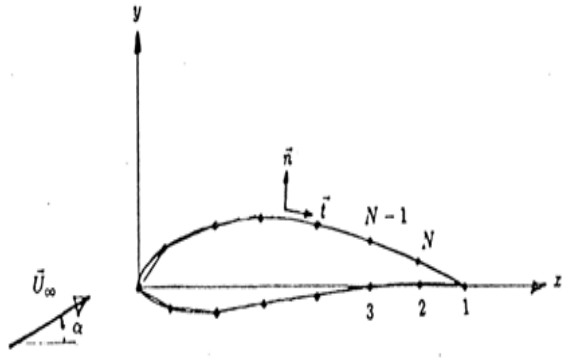

Figure 4. 2D foil schematic for viscous/inviscid interactive method.

The discretized equations for inviscid φ^i and φ^v viscous perturbation potential can be written as

$$\sum_{j=1}^{N} A_{ij}\varphi_j^i = \sum_{j=1}^{N} S_{ij}\left(\frac{\partial\varphi}{\partial n}\right) \tag{1}$$

$$\sum_{j=1}^{N} A_{ij}\varphi_j^v = \sum_{j=1}^{N} S_{ij}\left(\frac{\partial\varphi}{\partial n}\right)_j + \sum_{j=1}^{N+N_w} B_{ij}\sigma_j \tag{2}$$

where A and B are dipole and source influence coefficients and S is the blowing source (σ) influence coefficient representing the effect of viscosity.

The total potential on each body panel and wake is :

$$\Phi_i^v = \Phi_i^i + \sum_{j=1}^{N+N_W} H_{ij}\sigma_j \tag{3}$$

$$\Phi_{wake,i}^v = \Phi_{wake,i}^i + \sum_{j=1}^{N+N_W} G_{ij}\sigma_j \tag{4}$$

The viscous velocity or edge velocity is obtained by differentiation:

$$U_i^e = \frac{d\Phi_i^v}{ds} = U_i^{inv} + \sum_{j=1}^{N+N_W} D_{ij}\sigma_j \tag{5}$$

If there are N panels on the body and N_W panels in the wake then, in vector form

$$[U^e]_{(N+N_W,1)} = [U^{inv}]_{(N+N_W,1)} + [D]_{(N+N_W,N+N_W)}[\sigma]_{(N+N_W,1)} \tag{6}$$

The integral 2-D boundary layer equations for incompressible flow include the following standard integral momentum and the kinetic energy shape parameter equations:

Momentum equation

$$\frac{d\theta}{ds} + (2 + H - M_e^{\,2})\frac{\theta}{U_e}\frac{dU_e}{ds} = \frac{C_f}{2} \tag{7}$$

where Θ is momentum thickness, H is shape parameter, C_f is skin friction coefficient.

Kinetic energy equation

$$\theta\frac{dH^*}{ds} + (2H^{**} + H^*(1-H))\frac{\theta}{U_e}\frac{dU_e}{ds} = 2C_D - H^*\frac{C_f}{2} \tag{8}$$

where H^* is kinetic energy shape parameter, Θ^* is kinetic energy thickness, C_f is skin friction coefficient.

To close the integral boundary-layer equations (7) and (8), the following equations (Drela et al. 1994) are used for turbulent and laminar flows respectively.

Turbulent closure

$$\frac{\delta}{C_\tau}\frac{dC_\tau}{ds} = 5.6(C_{\tau EQ}^{\;0.5} - C_\tau^{\;0.5}) + 2\delta\left\{\frac{4}{3\delta^*}\left[\frac{C_f}{2} - \left(\frac{H_k - 1}{6.7H_k}\right)^2\right] - \frac{1}{U_e}\frac{dU_e}{ds}\right\}$$

Laminar closure

$$\frac{d\tilde{n}}{ds} = \frac{d\tilde{n}(H_k)}{d\,\mathrm{Re}_\theta}\frac{d\,\mathrm{Re}_\theta(H_k,\theta)}{ds}$$

2.3 Wall Transpiration Model in 3D

In 3D cases, the viscous edge velocity on each strip consists of the inviscid velocity plus the induced velocity by the blowing sources added on the same strip itself and the blowing sources on other strips as well. The 3-D interaction also leads to a velocity component induced due to the difference in the viscous and inviscid potentials at panels on other strips. Considering there are N panels on a strip and there are M such strips as shown in Fig. 5.

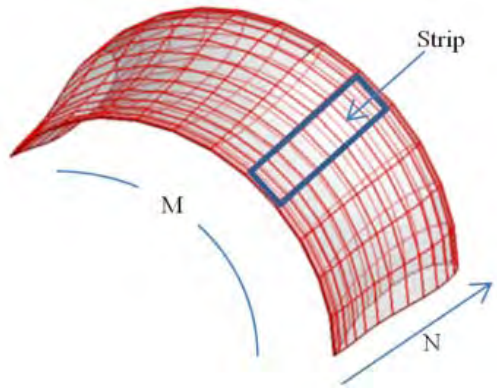

Figure 5. 3D duct geometry divided into 'M' strips each of 'N' panels.

The discretized equation for the perturbation potential on the panels of the K[th] strip can be written as

$$[A_{KK}]\varphi_K^{\,V} = [A_{KK}]\varphi_K^{\,i} + \sum_{j=1,j\neq K}^{M}[A_{Kj}]\left(\varphi_j^{\,i} - \varphi_j^{\,v}\right) + [B_{KK}]\sigma_K + \sum_{j=1,j\neq K}^{M}[B_{Kj}]\sigma_j \quad (9)$$

where A_{ij}, B_{ij} are each matrices of order NxN and subscripts i, j denote the influence of panels on the j[th] strip on the panels on the i[th] strip. σ_i, φ_i are vectors of order Nx1 for the i[th] strip,.

$$\varphi_K^{\,V} = \varphi_K^{\,i} + \sum_{j=1,j\neq K}^{M}[A_{KK}]^{-1}[A_{Kj}]\left(\varphi_j^{\,i} - \varphi_j^{\,v}\right) + [A_{KK}]^{-1}[B_{KK}]\sigma_K + \sum_{j=1,j\neq K}^{M}[A_{KK}]^{-1}[B_{Kj}]\sigma_j \quad (10)$$

The edge velocities are obtained by differentiating along the chordwise direction:

$$U_K^{\,V} = U_K^{\,i} + \sum_{j=1,j\neq K}^{M}[Q_K][A_{KK}]^{-1}[A_{Kj}]\left(\varphi_j^{\,i} - \varphi_j^{\,v}\right) + [Q_K][A_{11}]^{-1}[B_{11}]\sigma_1 + \sum_{j=2}^{M}[Q_K][A_{11}]^{-1}[B_{1j}]\sigma_j \quad (11)$$

The edge velocity expression can be written as:

where Q_K is the differentiation matrix on K^{th} strip

$$U_K^{\,V} = U_K^{\,i} + \sum_{j=2}^{M}[F_{Kj}]\left(\varphi_j^{\,i} - \varphi_j^{\,v}\right) + [D_{KK}]\sigma_K + \sum_{j=1,j\neq K}^{M}[D_{Kj}]\sigma_j \quad (12)$$

Note: The boxed term in the above expression for edge velocity was not included in the paper by Kinnas et al. (2012_3). The detailed derivation of the correction is given in Purohit (2013).

The second term on right hand side of above equation is the effect of potential difference due other strips; the third and fourth terms the induced velocity due to sources on the same strip and other strips respectively.

For the axisymmetric duct problem, the 2-D formulation of viscous-inviscid interaction for open duct case has been used by using the influence coefficients of an annular panel ring in place of the influence coefficients due to each panel.

2.4 Modification of Trailing edge

As discussed before, to apply potential based methods to ducts with blunt trailing edge, the trailing edge need to be modified. The location of the end point of the modified trailing edge and the horizontal location of the start of flap are given as parameters to find a flap shape satisfying the pressure equality condition at the actual trailing edge. The flap is modeled as a second order polynomial on both the lower and upper side as shown in Fig. 6. Since the pressures on the duct will vary with the advance ratio of the propeller, a different flap shape will be obtained for different advance ratios. This can also be confirmed from the streamlines of MPUF3A-RANS coupled simulations that indeed the recirculation region behind the duct is different for different blade rotational speeds.

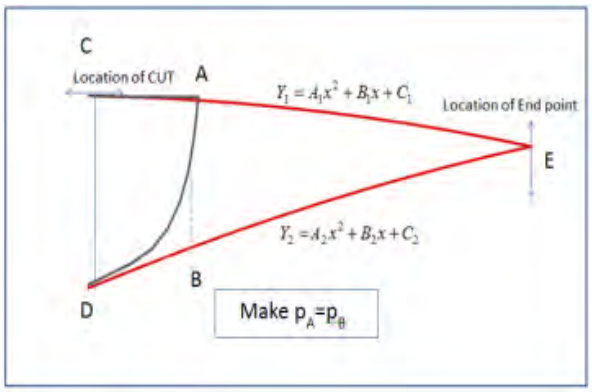

Figure 6. Extension of Blunt Trailing edge.

The method has been applied to an open blunt duct case and a ducted propeller for the design case of J=0.73 and the results are compared with MPUF3A/RANS simulations.

3 RESULTS AND DISCUSSION

3.1 Uniform Inflow

At first, the performance of the ducted propeller subject to a uniform inflow is investigated and then compared with the experimental measurements.

Figure 7 shows the geometry of blades, hub, and duct in the potential flow solver. The potential solver uses the image method for the duct and the inner surface of the duct is only used for analysis. The number of the panels of the key blade is 20 by 18. This propeller has four blades. The other blades also have the same number of panels with that of the key blade. The wake is generated with the simplified alignment based on the velocity of the trailing edge. The hub is considered infinite.

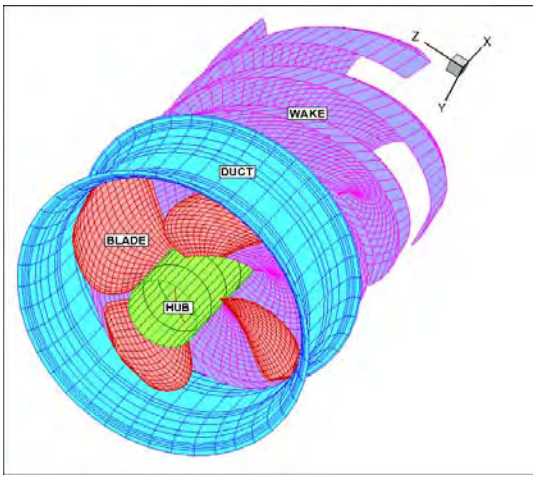

Figure 7. Geometry of the potential solver.

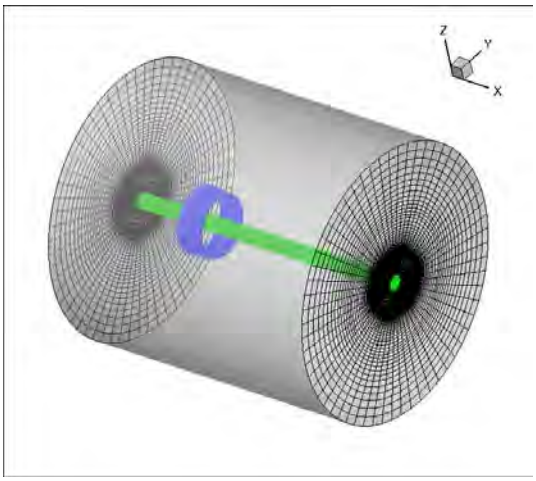

Figure 8. Geometry of the viscous fluid flow solver.

Figure 8 represents the geometry of the viscous fluid flow solver. In order to make the running condition close to the potential flow solver, the infinite hub is considered. This kind of consideration can improve the quality of the three-dimensional mesh at the center. This three dimensional mesh is generated by revolving the axisymmetric mesh. Thus the error due to the difference of mesh between axisymmetric and three dimensional runs can be minimized. The three dimensional mesh has 60 nodes in the circumferential direction. This number is the same with that of the potential flow in time-averaging.

The propeller only case is tested subject to a uniform inflow without any iteration procedure. Since the normalized inflow condition is set to 1.0, the effective wake should be able to recover this value. Figure 9 shows the result of the coupling. 'UXE' means the axial component of the effective wake. It is distributed close to the inflow condition over the blade. Most of the control points show the errors are less than 3% except a couple of control points near the tip downstream.

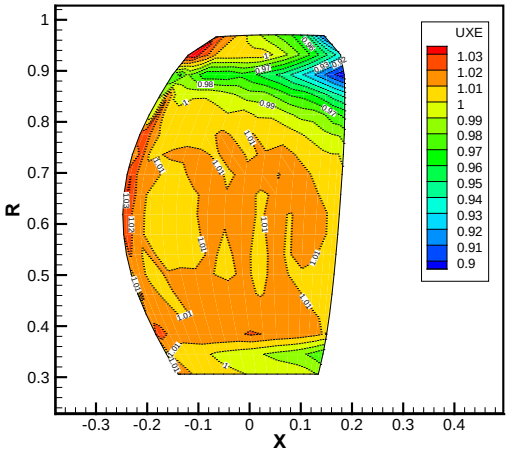

Figure 9. Axial effective wake of the propeller only case (3X), in the case of uniform inflow.

The effective wakes of the ducted propeller in the cases of axisymmetric and three dimensional run are shown in the figures 10 and 11, respectively. In the both figures, UXE means the axial effective wake. The normalized inflow velocity far upstream is 1.0. The inflow is accelerated by the presence of the duct. The acceleration of the flow can be observed in the figures. The area near the duct shows the strong acceleration. The result of the three dimensional case is close to that of the axisymmetric case, as expected.

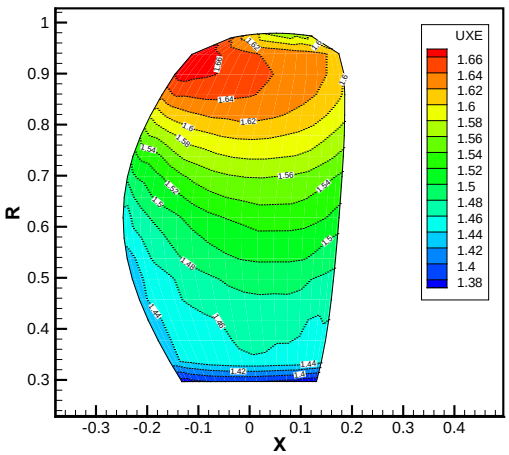

Figure 10. Axial effective wake of the ducted propeller case (3X), in the case of uniform inflow.

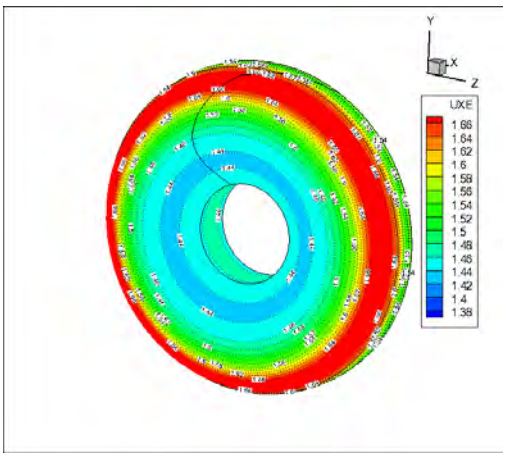

Figure 11. Axial effective wake of the ducted propeller case (3D), in the case of uniform inflow.

In Figure 12, the performance of the ducted propeller is compared with the experimental measurement that was carried out by HSVA and presented by Kinnas et al (2012_1). KT, KTD, and 10KQ represent the propeller thrust, the duct thrust, and the torque, respectively. The line with the filled circle in black is the experimental data. The circle is the result of the coupling method. The performance predicted by the coupling of potential flow solver (MPUF-3A) and a viscous fluid flow solver is in very good agreement with the experimental measurement in a large range. The result from PROPCAV using the modified trailing edge obtained from the extension scheme is also plotted for J=0.73.

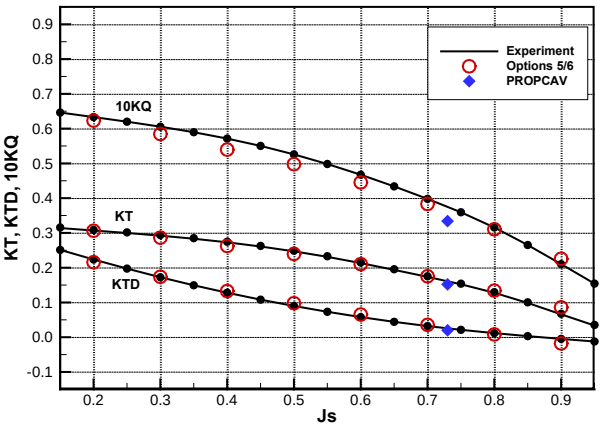

Figure 12. Comparison of the performance between numerical results and experimental measurements.

3.2 Ducted Propeller in Uniform and Inclined Inflow

The proposed methods were also applied to a ducted propeller under uniform and inclined inflow, as shown in Fig. 13. In this case, the effective wake varies in both circumferential and axial direction in the propeller zone, thus the fully 3D option in the methods is enabled. In other words, the effective wake is calculated at all control points and all blade angles. In the RANS simulation of the hybrid method, 1.3 million hexahedral cells were used to mesh the domain. Standard $k-\epsilon$ turbulence model was adopted. In the VLM, 20x18(chordwise x spanwise) panels were used to discretize the propeller blades.

Two different angles of inclination of the inflow (10degree, and 15 degree) were analyzed. For each inflow condition, the total wall time for 7 iterations between the RANS and the VLM was about 11 hours on 16 Intel Xeon 2.50GHz cores.

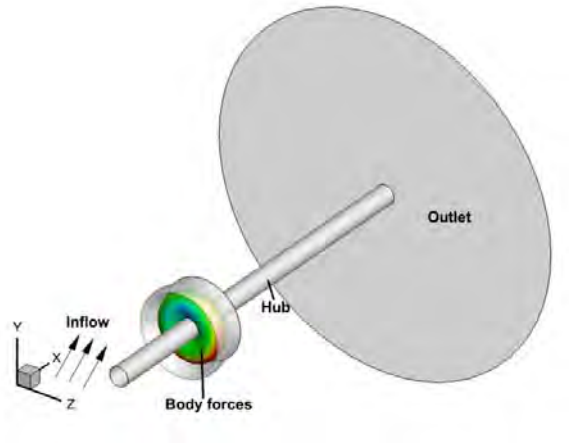

Figure 13: Schematic plot for the case of a ducted propeller under inclined and uniform inflow.

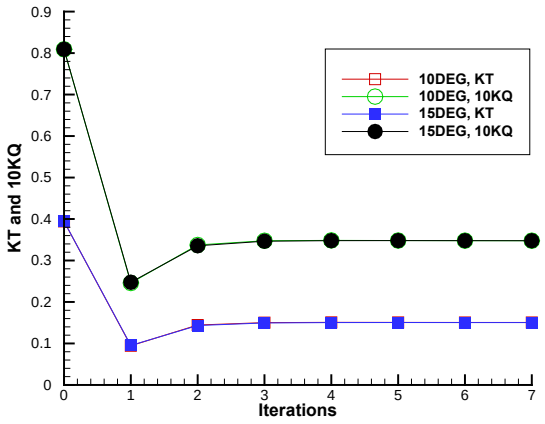

Figure 14: Convergence history of averaged KT and KQ.

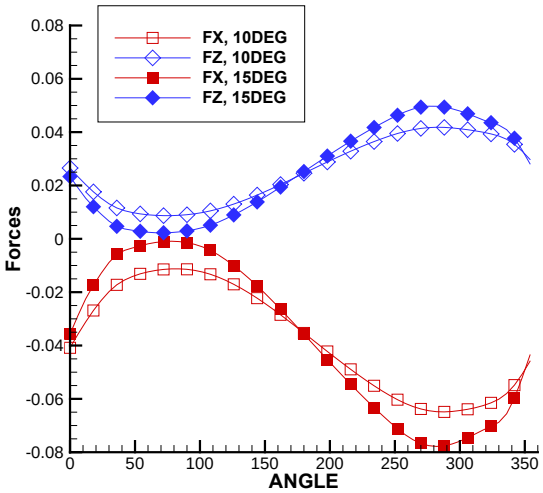

Figure 15: Comparison of the unsteady forces between the two different inflow conditions.

Fig. 14 shows the convergence history of the averaged KT and KQ. Obviously the simulation converged in the 3rd iteration. The averaged KT and KQ for the two different inflow conditions are very close to each other. This is because the presence of the duct straightens the flow to some extent. Fig. 15 compares the unsteady blade forces between the two different inflow conditions. Clearly the higher the angle of inclination is, the stronger the blade forces vary in time. Fig. 16 shows the predicted effective wake at $x = 0$ plane. In this figure, 'UXE' means the axial effective wake. As expected, although the flow patterns for the two different inflow condition are similar, the 15DEG inflow inclination results in stronger transverse flow components.

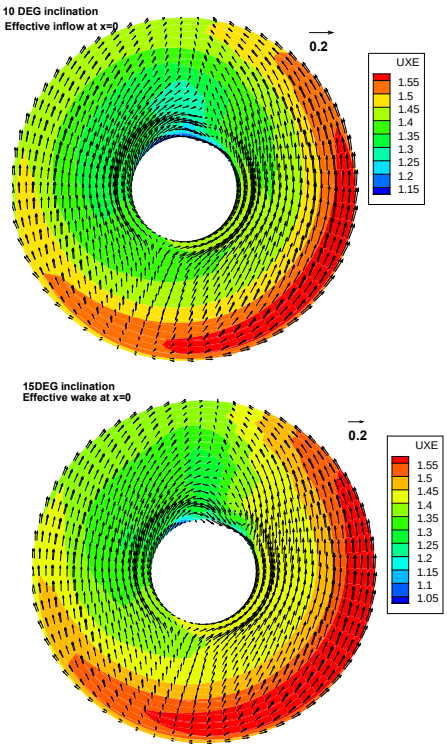

Figure 16. Predicted axial effective wakes at x=0 plane. Top: 10DEG inflow inclination; Bottom: 15DEG inflow inclination.

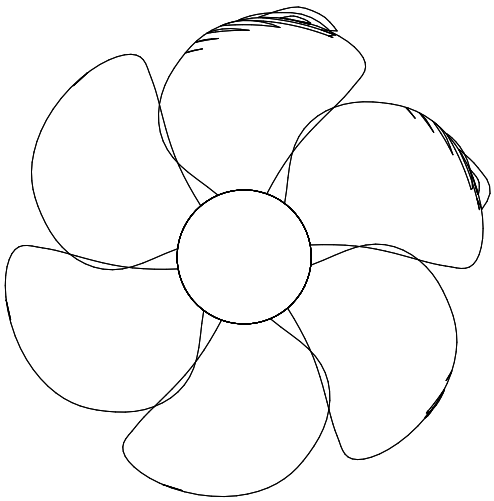

Figure 17. Predicted cavity pattern at 10 DEG angle of inclination of the inflow, in the case of ducted propeller.

Fig. 17 shows the predicted cavity pattern. The appearance of the cavities is consistent with the time history of the unsteady blade forces.

3.3 Viscous-Inviscid interaction: Duct only case

To verify the application of the viscous-inviscid interactive scheme using annular influence coefficients, the results obtained from the scheme were compared with those obtained from RANS. Two cases, one for duct with a sharp trailing edge and one for duct with a blunt trailing edge have been presented. For the case of duct with blunt trailing edge, the extension scheme as described previously has been used to get the flap shape and the modified shape is used in the viscous-inviscid interactive scheme

3.3.1 Sharp Trailing edge (Long duct)

The 3D viscous/inviscid interactive method is applied to a bare duct case. The DTMB duct analyzed had a NACA66 thickness form, with a maximum thickness-chord ratio t_{max}/C = 0.1. The camber has a NACA a = 0.8 mean distribution and the maximum camber-chord ratio is f_{max}/C = 0.04. The chord length is 4 and the inner radius of duct is 1. The duct geometry is shown in Fig. 18. A duct with a longer chord was selected because the difference in viscous and inviscid pressures was more prominent for a longer chord.

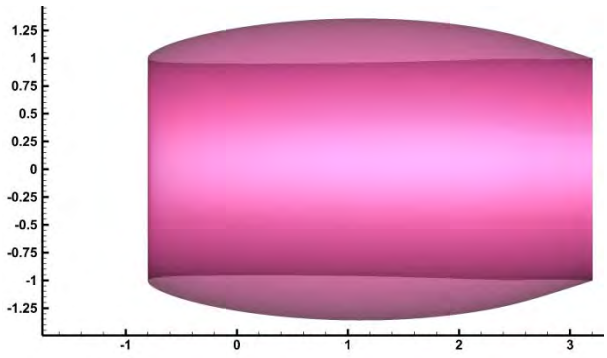

Figure 18. Geometry of the long duct.

The pressure obtained from the viscous-inviscid interactive method is in very good agreement with that obtained from RANS as shown in Fig. 19.

The displacement thickness on lower side and upper side of duct was calculated from the velocity profiles obtained from RANS simulation, A very fine grid with $y^+ \sim O(1)$ was generated to get an accurate velocity profile. The displacement thickness obtained from the viscous-inviscid interactive method is in good agreement with that obtained from RANS as shown in Fig. 20 and 21.

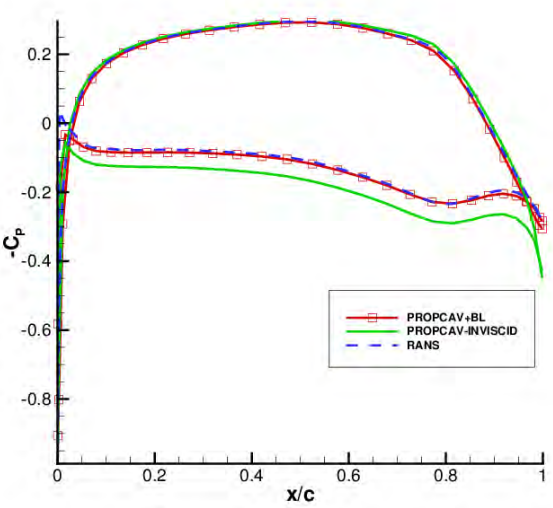

Figure 19. Comparison of pressure coefficient between RANS, inviscid panel method and viscous-inviscid interactive method.

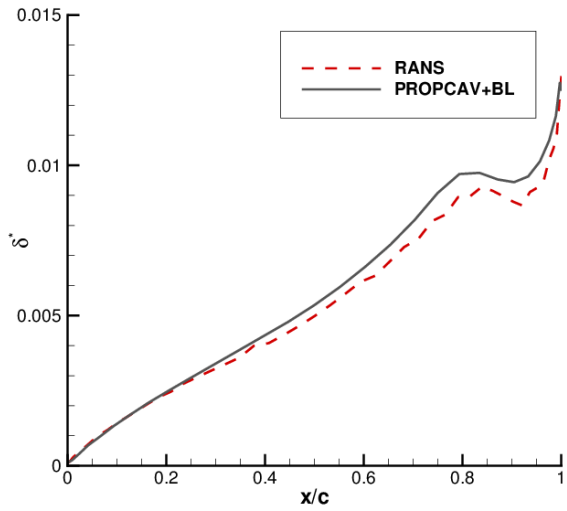

Figure 20. Comparison of displacement thickness on lower side of 'long' duct.

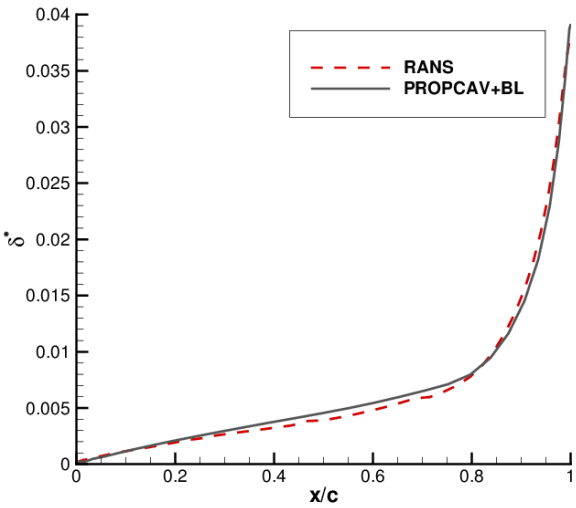

Figure 21. Comparison of displacement thickness on upper side of 'long' duct.

3.3.2 Blunt Trailing edge

The extension scheme described above was applied to get the modified shape of duct and the viscous-inviscid method was applied on the modified shape. The actual shape and modified shape are shown in Fig. 22. The chord length "c" of the actual duct is 1. The streamlines obtained from the RANS simulation and the duct geometry near the trailing edge location are shown in Fig. 23. The pressure obtained from the viscous-inviscid interactive method applied to the modified duct shape is in good agreement with that obtained from RANS for the actual duct shape as shown in Fig. 24. Thus the interactive scheme is able to predict the deviation from the inviscid pressure on the duct.

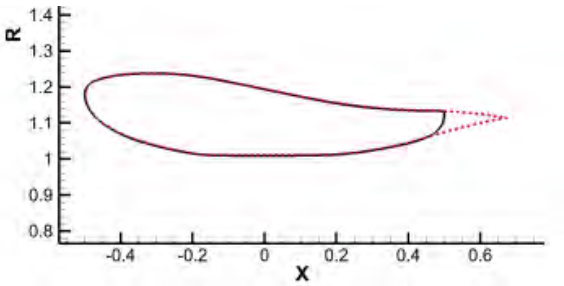

Figure 22. Geometry of duct with blunt trailing edge and extension.

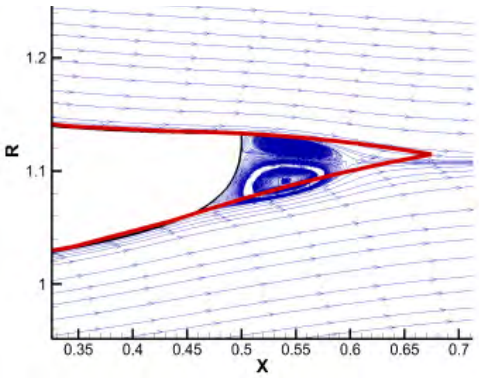

Figure 23. Streamlines along the duct and geometry of duct with extension near trailing edge.

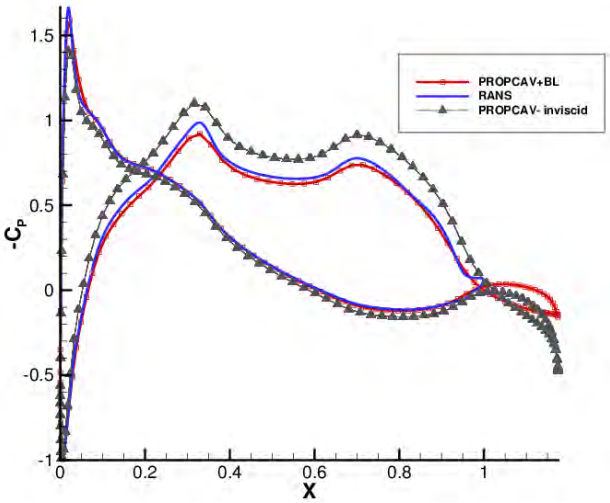

Figure 24. Comparison of pressure coefficient between RANS, inviscid panel method and viscous-inviscid interactive method.

The displacement thickness obtained from the viscous-inviscid interactive method is in good agreement with that obtained from RANS as shown in Figures 25 and 26 which shows that the extended shape can provide reasonable results.

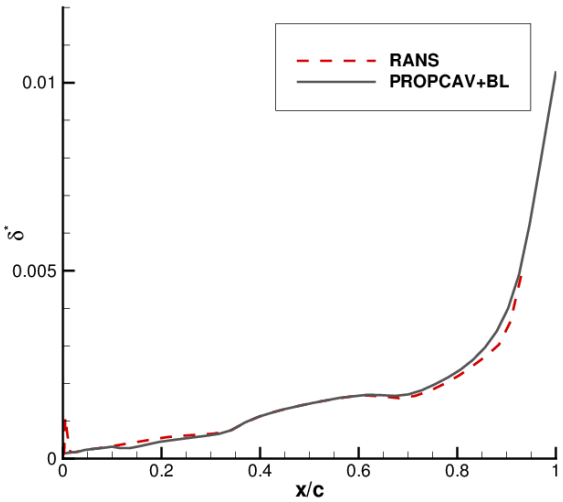

Figure 25. Comparison of displacement thickness on lower side of duct.

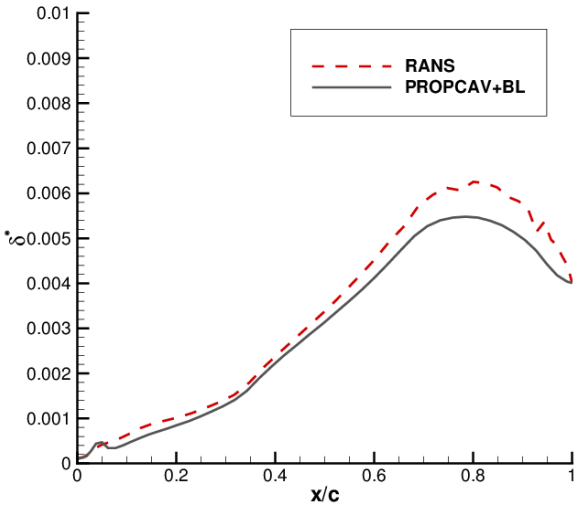

Figure 26. Comparison of displacement thickness on upper side of duct.

3.4 Trailing edge modification-Ducted propeller case

The ducted propeller case is run for a duct with a blunt trailing edge. The extension scheme as described previously is applied for the case of J=0.73. The circumferentially averaged mean pressures on the duct upper and lower sides are required to match at the actual trailing edge location to find the extension shape. PROPCAV is applied on the modified duct geometry obtained using the extension scheme. The circumferentially averaged pressure on duct from PROPCAV applied to extended duct shape is compared with the pressure from MPUF3A/RANS for the actual duct shape and shown in Fig. 27. The actual duct trailing edge is at x=0.5 in Fig. 27. In addition the predicted forces are shown in Fig. 12.

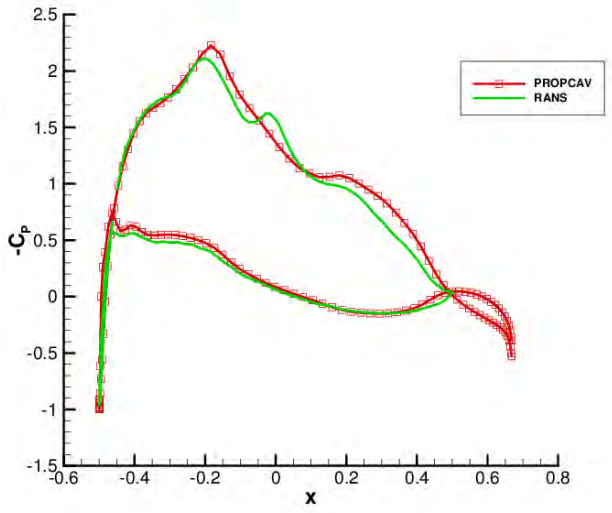

Figure 27. Comparison of pressure coefficient on duct for J=0.73.

4 CONCLUSIONS AND FUTURE WORK

In this paper, a ducted propeller subject to uniform and inclined inflow is investigated. The hybrid numerical methods coupling the potential flow solver and the viscous fluid flow solver are used to predict the performance of the ducted propeller.

For the propeller only case, the effective wake shows good agreement with the inflow over the blade except at a few control points. The effective wake of the ducted propeller can simulate the acceleration of the flow by the presence of the duct.

The performance of the ducted propeller by the hybrid method is compared with experimental data. The results are found to be in good agreement with measurements over a large range of the operating conditions.

ACKNOWLEDGMENTS

Support for this research was provided by the U.S. Office of Naval Research (Contract N00014-07-1-0616) and Phases VI of the "Consortium on Cavitation Performance of High Speed Propulsors" with the following current members: American Bureau of Shipping, Kawasaki Heavy Industry Ltd., Rolls-Royce Marine AB, Rolls-Royce Marine AS, SSPA AB, Andritz Hydro GmbH, Wärtsilä Netherlands B.V., Wärtsilä Norway AS, Wärtsilä Lips Defense S.A.S., and Wärtsilä CME Zhenjiang Propeller Co. Ltd. .

REFERENCES

Drela, M., and Giles, M. B. (1987) "ISES: A Two-dimensional Viscous Aerodynamic Design and Analysis Code." Technical Report, AIAA 87-0424.

Hufford, G. S., Drela, M., and Kerwin, J. E. (1994) "Viscous flow around marine propellers using boundary-layer strip theory." J. Ship Res, vol 38(1):52–62.

Hughes, MJ, Kinnas, SA & Kerwin, JE (1992). 'Experimental Validation of a Ducted Propeller Analysis Method'. J. Fluids Eng.-Trans. ASME, 114(2), pp 214-219.

Kerwin, J. E., and Lee, C. S.(1987) "Prediction of steady and unsteady marine propeller performance by numerical lifting surface theory." Transactions SNAME, vol 86.

Kerwin, JE, Keenan, D, Black, S. & Diggs, J (1994). 'A Coupled Viscous/potential Flow Design Method for Wake-adapted, Multi-stage, Ducted Propulsors using Generalized Geometry. Discussion. Authors' Closure'. Trans. SNAME, 102, pp 23-56.

Kinnas, S. A., Lee, HS., Gu, H. & Gupta, A. (2004). 'Prediction of Performance of Ducted and Podded Propellers'. Proceedings of the 25th Symposium on Navel Hydrodynamics, St. John's, Newfoundland and Labrador, Canada.

Kinnas, S. A., Chang, S.-H., Yu, Y.-H. & He, L. (2009). 'A Hybrid Viscous/Potential Flow Method for the Prediction of the Performance of Podded and Ducted Propellers.'. Proceedings of Propeller/Shafting '09 Symposium, Verginia Beach, VA, USA.

Kinnas, S. A., Chang, S.-H., Tian, Y. & Jeon, C.-H. (2012_1). 'Steady and Unsteady Cavitating Performance Predicition of Ducted Propulsors'. Proceedings of the 22nd Conference of the International Society on Offshore and Polar Engineers – ISOPE2012, Rhodes, Greece.

Kinnas, S. A., Jeon, C.-H. & Tian, Y. (2012_2). 'A Hybrid Viscous/Potential Flow Method for the Prediction of the Wetted and Cavitating Performance of Ducted Propellers'. SNAME Propellers/Shafting Symposium 2012 , VA, USA.

Kinnas, S. A.,Yu, X. & Tian, Y. (2012_3) "Prediction of Propeller Performance under High Loading Conditions with Viscous/Inviscid Interaction and a Full Wake Alignment Model." 29th symposium on Naval Hydrodynamics, Sweden.

Pan, Y. (2009) "A viscous/inviscid interactive approach and its application to hydrofoils and propellers with non−zero trailing edge thickness." M.S. Thesis, Ocean Engineering Group, University of Texas at Austin.

Purohit, J. (2013) "Viscous-Inviscid interactive method applied to Ducted Propellers." M.S. Thesis (under preparation) , Ocean Engineering Group, University of Texas at Austin.

Sun, H. (2008) "Performance Prediction of Cavitating Propulsors Using a Viscous/ Inviscid Interaction Method," PhD Thesis, Ocean Engineering Group, University of Texas at Austin.

Yu X. (2012) "Three Dimensional Viscous/Inviscid Interactive Method and Its Application to Propeller Blades." M.S. Thesis, Ocean Engineering Group, University of Texas at Austin.